An improved model for N_2 adsorption on graphitic adsorbents and graphitized thermal carbon black—The importance of the anisotropy of graphene

Luisa Prasetyo, Shiliang (Johnathan) Tan, Yonghong Zeng, D. D. Do, and D. Nicholson

Citation: The Journal of Chemical Physics **146**, 184702 (2017); doi: 10.1063/1.4982926
View online: https://doi.org/10.1063/1.4982926
View Table of Contents: http://aip.scitation.org/toc/jcp/146/18
Published by the American Institute of Physics

An improved model for N_2 adsorption on graphitic adsorbents and graphitized thermal carbon black—The importance of the anisotropy of graphene

Luisa Prasetyo, Shiliang (Johnathan) Tan, Yonghong Zeng, D. D. Do,[a] and D. Nicholson
School of Chemical Engineering, University of Queensland, St. Lucia, Queensland 4072, Australia

(Received 7 March 2017; accepted 19 April 2017; published online 11 May 2017)

Computer simulations of N_2 adsorption on graphite frequently use the 10-4-3 equation with Steele's molecular parameters to describe the dispersive-repulsive interaction between a molecule and graphite. This model assumes that graphite is a uniformly homogeneous continuum solid, and its derivation implies the following assumptions: (1) the solid is built from stacked, equally spaced graphene layers, (2) there is an infinite number of layers, and (3) the carbon atom molecular parameters are invariant for all layers (collision diameter of 0.34 nm and reduced well depth of interaction energy of 28 K). Despite the fact that this model can give an acceptable description of experimental data for this system, there are experimental observations that simulation results fail to account for. First, the isotherm does not exhibit a step in the sub-monolayer coverage region at 77 K, which is attributed to a transition from the supercritical state of the adsorbate to the commensurate state, and therefore fails to reproduce the cusp and heat spike in the experimental isosteric heat curve versus loading at close to monolayer coverage. Second, the simulation results overpredict the experimental data in the multilayer region. These discrepancies suggest that (1) the absence of lateral corrugation in the 10-4-3 potential misses the commensurate to incommensurate transition and (2) the long-range solid-fluid potential, experienced by the second and higher layers onwards, is too strong. Here we examine a revised graphite potential model that incorporates three features absent from the 10-4-3 model: (1) an energetic corrugation of the potential arising from the discrete atom structure of the adsorbent, (2) the unequal spacing of the graphene layers due to the anisotropic force field acting on graphene layers at the surface, and (3) the different polarizabilities of carbon atoms in graphite, parallel and normal to the graphene surface. These features are corroborated by a number of experimental measurements and quantum-mechanical calculations: (1) the Low-Energy Electron Diffraction (LEED) and Surface-Extended X-ray Absorption Fine Structure (SEXAFS) experiments show that the first adsorbate layer is smaller than predicted by the 10-4-3 model with the traditional molecular parameters suggested by Steele, and (2) the potential well depth for atoms in graphene is stronger than for C-atoms in graphite. The simulation results using this revised graphite model give an improved description of the fine features of adsorption of N_2 on graphite: the sub-step in the first layer of the isotherm, the spike in the isosteric heat curve versus loading, and the coverage at higher loadings. *Published by AIP Publishing.* [http://dx.doi.org/10.1063/1.4982926]

I. INTRODUCTION

Computer simulation studies of adsorption of gases on graphite using the homogeneous continuum 10-4-3 model[1] have been used to investigate the mechanism of adsorption for a number of single and multisite molecules, for example, argon,[2–4] methane,[5] krypton,[6,7] nitrogen,[8,9] carbon dioxide,[10] benzene,[11] ethane,[12] ethylene,[12] propylene,[13] carbon tetrachloride,[14] n-butane, n-pentane, n-hexane,[15] methanol,[16,17] ethanol,[17] and ammonia.[18] This model assumes that graphite is a uniformly homogeneous continuum solid, and its derivation implies the following assumptions: (1) the solid is built from stacked, equally spaced graphene layers, (2) there is an infinite number of layers, and (3) the carbon atom molecular parameters are invariant for all layers (collision diameter of 0.34 nm and reduced well depth of interaction energy of 28 K[19]). Despite the fact that this model can give an acceptable description of experimental data for the aforementioned systems, there are experimental observations that simulation results fail to account for, i.e., the adsorption of N_2 on graphite at its boiling point of 77 K,[1,2] which is commonly used as a reference for surface area determination and the analysis of pore size distribution. To fully describe N_2 adsorption with the molecular simulation, we need to account for its molecular shape and quadrupole. Even simulations that include these refinements[3,8,9] fail to register several experimental observations[20–23] including (1) the sub-step in the isotherm, associated with the transition from a supercritical 2D fluid to a commensurate solid; (2) the cusp and spike in the isosteric heat curve close to monolayer coverage; (3) the correct second and higher layer coverage, which is overpredicted in simulations.

Interestingly, when N_2 is modelled as a single Lennard-Jones (LJ) site, a sub-step in the simulated isotherm is

[a] Author to whom correspondence should be addressed. Electronic mail: d.d.do@uq.edu.au

observed,[9] contradicting the expectation that a physically superior two-site LJ site model for N_2 with three partial charges would perform better. Since a multisite model of N_2 gives an excellent account of vapour-liquid equilibria and the interfacial tension of the bulk phase,[24] the onus is now placed on the validity of the widely used 10-4-3 model for the graphite potential energy field in which an implicit assumption is that graphene layers are equally spaced. Ustinov recently raised this question[25] and argued that the collision diameter of the carbon atom (σ_{CC}) in a graphene layer should be smaller than the value of 0.34 nm first proposed by Steele.[19] Ustinov's argument is based on the observation that when the C-collision diameter is reduced to 0.26 nm, the potential profile of an atom interacting with the solid (Solid-Fluid (SF) potential) decays faster with distance from the graphite surface, resulting in a weaker SF potential at the position of the second layer and an improved description of higher layer adsorption. Furthermore, when σ_{CC} is smaller, an atomically discrete model of the surface is more energetically corrugated, and simulations at 77 K show a transition from a supercritical 2D fluid to commensurate packing, as a sub-step in the isotherm and a spike in the heat curve versus loading. However, this choice of 0.26 nm was implied for all layers in the graphite, which is in disagreement with the accepted X-ray diffraction (XRD) data which give an interlayer spacing in a graphite of 0.3354 nm, and the fact that the distance of the first adsorbate layer from the surface is greater than predicted by Ustinov's model.[26,27]

The potential from the proposed model is used here for a comprehensive study of N_2 adsorption over a range of temperatures. This study highlights the differences between the proposed model and the 10-4-3 continuum graphite model, especially at low temperatures where the corrugation is more strongly manifested, and demonstrates the improved agreement between simulation results using this model and experimental data. The anisotropy of polarizability in the first graphene layer also accounts for a shift in the 2D-transition for the first two adsorbed layers and the sub-steps in the isotherm, associated with the spike in the plot of the isosteric heat versus loading. By decomposing the isotherm and the isosteric heat into contributions from the first and second layers, we elucidate the mechanisms underlying these transitions.

II. THEORY

A. A new molecular model for graphite

In this work, we propose a revised molecular model for graphite that incorporates the following important features absent from the homogeneous continuum solid 10-4-3 model:

1. Recent density functional theory (DFT) theoretical studies by Gobre and Tkachenko[28] suggest that the van der Waals attractive parameter for C may be larger in the first layer than the generally accepted value of 28 K. Here we have used 35 K for this parameter in calculating interactions with the outermost (top) graphene layer.
2. Low-Energy Electron Diffraction (LEED) and Surface-Extended X-ray Absorption Fine Structure (SEXAFS) experiments[26,27] indicate that the collision diameter for carbon in the top graphene layer must be smaller than 0.34 nm. This implies that the interlayer spacing between the first layer and the rest of the solid is less than the inter-layer spacing in bulk graphite measured experimentally by X-ray diffraction (XRD). We postulate that this reduction in layer spacing occurs because the outside layer(s) experiences forces from the underlying graphite which are not balanced by any forces from the other side. The interlayer spacing below the top two layers must be 0.3354 nm and the well depth of carbon atom of graphene layers below these layers 28 K in order to give the correct value for the compressibility of graphite.
   In this work, the equilibrium interlayer spacings were determined by minimising the potential energy as follows. The graphite surface was modelled as a stack of layers, infinite in the x- and y-direction parallel to the surface. The uppermost layer was modelled as one Crowell[29] layer while the underneath layers were modelled by the 10-4-3 potential. The spacing between the two top layers, calculated by either the minimization of energy or Monte Carlo simulation under vacuum, was found to be smaller than the underlying layers as shown in the illustration (Fig. 1). From the position of the minimum in the interaction between the top layer and the 10-4-3 solid, we find an equilibrium spacing between the top two layers of $\Delta 1 = 0.2987$ nm. The molecular parameter σ_{CC}, for a carbon atom in the first layer, was therefore set as 0.28 nm and $\varepsilon_{CC}/k_B = 35$ K. The smaller σ_{CC} was calculated based on the LEED experimental result for argon[30] by the Lorentz-Berthelot mixing rule, while $\varepsilon_{CC}/k_B = 35$ K was chosen by matching the simulated Henry constant[31] with the experimental Henry constant. For consecutive layers, $\sigma_{CC} = 0.34$ nm and $\varepsilon_{CC}/k_B = 28\ K$ were used. The surface density of carbon in the graphene layer is 38.2 nm^{-2} while the cross-collision diameter and the well-depth of the solid-fluid interaction energy were calculated by the Lorentz-Berthelot mixing rule.
3. The discrete atom structure of graphite implies different adsorption energies at different site locations on the graphite surface[32] and also the effect of the anisotropy of polarisability, parallel and normal to the surface.[26,27]

B. Grand Canonical Monte Carlo (GCMC) simulations

In the Grand Canonical Monte Carlo (GCMC) simulations, we used 150 000 cycles for both equilibration and sampling stages. Each cycle consisted of 1000 attempted

FIG. 1. Schematic illustration of solid arrangement of graphite. Top layer is modelled as a corrugated Crowell surface while the bottom layer is modelled as the Steele surface of infinite layers.

TABLE I. Lennard-Jones molecular parameters and partial charges of N_2.[24]

Species	Site	X (nm)	Y (nm)	Z (nm)	Collision diameter σ (nm)	Reduced well depth (K)	q (e)
Nitrogen	N	0.055	0	0	0.331	36	–0.482
	N	0.055	0	0	0.331	36	–0.482
	...	0	0	0	0	0	0.964

displacement, insertion, and deletion moves, chosen with equal probability. In the equilibration stage, the maximum displacement step length was initially set as 2 nm and was adjusted at the end of each cycle to give an acceptance ratio of 20%. The lengths of the simulation box in the *x*- and *y*-direction were $(30 \times 15\sqrt{3})\ a_{Gr}$ to ensure the periodicity of the graphite surface, where a_0 is the graphite lattice constant (a_{Gr} = 0.246 nm). The dimension in the *z*-direction was 2 nm. The graphite surface was infinite in the x and y directions (modelled with periodic boundary conditions), and the atom centres in the uppermost graphene layer of the graphitized thermal carbon black (GTCB) were positioned at z = 0 and a hard wall was positioned at z = 2 nm.

C. Fluid-fluid and solid-fluid potentials

1. Fluid-fluid (FF) potential

The interaction between two N_2 molecules (Fluid-Fluid (FF) interaction) is constructed from the two 12-6 Lennard-Jones sites with three fixed partial charges. The two LJ sites are located at the centres of the N_2 atoms and the charges reside on the axis joining the two nitrogen atoms, with the two negative charges on the centres of the nitrogen atoms and one positive charge at the middle point on the axis. This 2LJ + 3q model, proposed by Potoff and Siepmann,[24] is denoted as the Transferable Potentials for Phase Equilibria Force Field (TraPPE) model; its molecular parameters are listed in Table I. The magnitudes and the positions of these three charges are chosen to reproduce the quadrupole moment of N_2. The elongated shape of N_2 provides an opportunity to study how the structure of the adsorbate on the surface is balanced by the interaction energy among N_2 molecules and the interaction energy between N_2 molecules and the energetically corrugated graphite surface. On the one hand, the molecule-molecule interaction between N_2 molecules favours a T-arrangement; on the other hand the SF interaction favours an in-registry arrangement between the centre of mass (COM) of N_2 with the energetically corrugated surface. This interplay results in a transition from one state of the adsorbate to another state and will be further discussed in Sec. III.

2. Solid-fluid (SF) potential

The corrugation in the solid-fluid (SF) interaction is accounted for in the uppermost graphene layer, using the equation given by Kim and Steele[33] (for the sake of completeness we present their equation in Subsection 1 of the Appendix as Eq. (A1)). The SF interaction from the deeper layers is described by the standard 10-4-3 equation[1] assuming that the rest of the adsorbent can be approximated as a continuum solid. The energetic corrugation of the potential function parallel to the surface planes is also modified by the difference in the carbon atom polarizability parallel to the surface and normal to the surface (see, for example, the works of Carlos and Cole[26,27] and Nicholson[34]) which enhances the energetic corrugation. Carlos and Cole[27] introduced two parameters γ_A and γ_R to account for the anisotropy of polarisability. The parameter γ_A comes from the product of the dipole coupling tensors that appear in the calculation of the dispersion force term and depends on the ratio of parallel to normal polarisability components of the polarisability tensor; various estimates suggest a value in the range 0.25 to 0.4.[35] The parameter γ_R does not have any recognised physical basis and was introduced by Carlos and Cole as a fitting parameter to give agreement with beam scattering data for helium for which they found $\gamma_R = -0.29$. Joshi and Tildesley[42] applied the theory of Carlos and Cole to the analysis of N_2 adsorption on graphite and found a value of $\gamma_R = -1.05$. In this work we have adopted values of $\gamma_A = 0.4$ and $\gamma_R = -1.05$ for these parameters. The SF potential contour plot of the modified model is shown in Fig. 2.

To show the difference between the SF potential calculated with the current model and the 10-4-3 potential, we present plots of their z-dependence with anisotropy (Figs. 3(a)

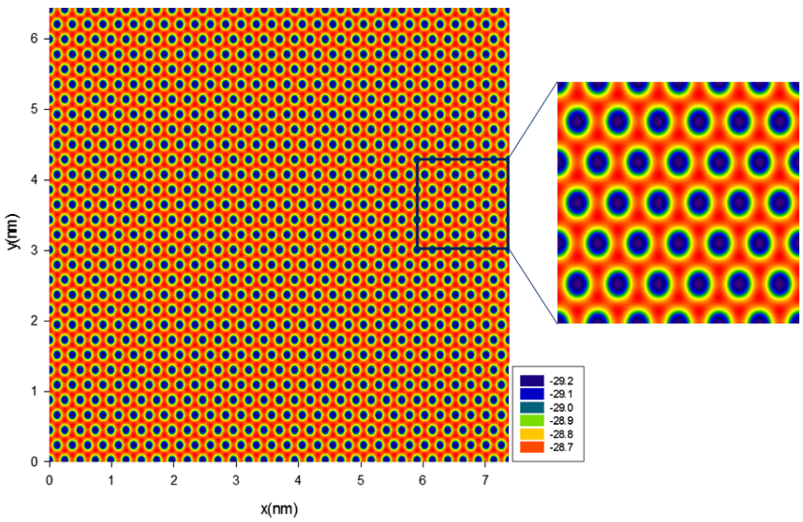

FIG. 2. SF potential contour plot obtained with the revised model. The size of the box in the *x*- and *y*-direction is $30 \times 15\sqrt{3}\ a_0$ to ensure the periodicity of the graphite surface.

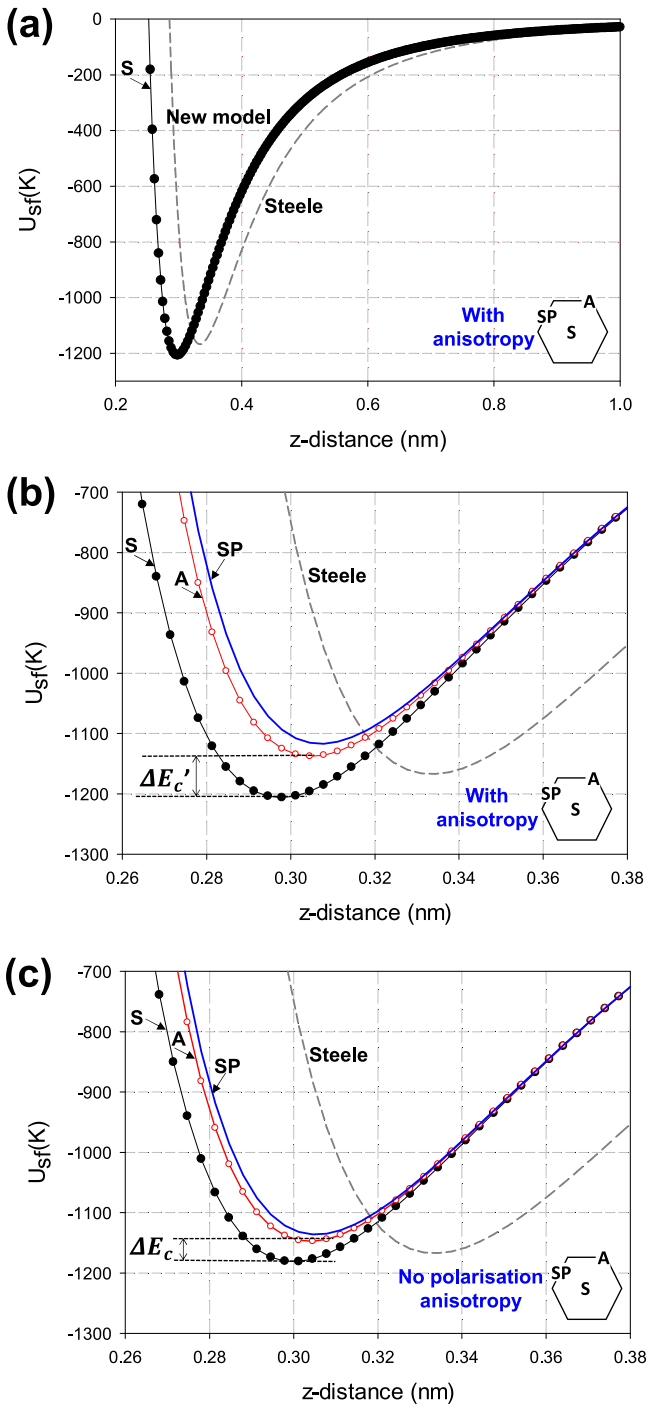

FIG. 3. Comparison between the SF energy profile of N_2 with a 10-4-3 potential model using the molecular parameters suggested by Steele and the new model: (a) and (b) with anisotropy (the enlarged scale is shown in (b)), (c) no polarisation anisotropy. The corrugation energy is defined as the difference between the two minima of the SF potentials corresponding to the centre of the hexagon and the top of the carbon atom.

and 3(b)) and without (Fig. 3(c)). As expected the minimum in the SF potential is shifted closer to the surface, from 0.3354 nm to 0.2987 nm. This is supported by LEED measurements for Ar, Kr, and Xe which show that these species are closer to the graphite surface[30] than 0.335 nm. Second, the SF interaction for the new model decays faster than the 10-4-3 potential (Fig. 3(a)) and therefore gives better agreement with experiment at higher loading. Third the corrugation energy in the presence of anisotropy ($\Delta E_c'$) is 1.5 times greater than that in the absence of anisotropy (ΔE_c) which is equal to the empirical factor introduced by Kim and Steele.[33]

D. Thermodynamic properties

1. Surface excess

The surface excess concentration is defined as

$$\Gamma_{ex} = \frac{N_{ex}}{L_x L_y} = \frac{\langle N \rangle - V_{acc}\rho_G}{L_x L_y}, \quad (1)$$

where N_{ex} is the excess amount adsorbed, $\langle N \rangle$ is the ensemble average of the number of particles in the simulation box, ρ_G is the bulk gas density, V_{acc} is the accessible volume (defined as the volume that is accessible to the center of a molecule, where the SF potential is non-positive), L_x and L_y are the box dimensions in the x- and y-direction, respectively.

2. Isosteric heat

The isosteric heat was calculated from fluctuation theory[36] as

$$q_{st} = \frac{\langle U \rangle \langle N \rangle - \langle UN \rangle}{\langle N^2 \rangle - \langle N \rangle^2} + k_B T, \quad (2)$$

where U is the sum of the potential energies of interaction between adsorbate molecules (U_{FF}) and between adsorbate-solid adsorbent (U_{SF}), and N is the number of particle in the system.

To understand how various interactions contribute to the isosteric heat, we decomposed the energy term in the above equation into contributions from the SF and FF interactions. Similarly, the contributions from each layer, U_K, can be calculated from

$$q_K = \frac{\langle U_K \rangle \langle N \rangle - \langle U_K N \rangle}{\langle N^2 \rangle - \langle N \rangle^2}, \quad (3)$$

where U_K is the energy calculated as the sum of pairwise energies when two molecules reside in the same layer or half the pairwise energy if one of them is located in a different layer. The sum of contributions from all layers is thus the total isosteric heat.

3. Local density distribution (LLD)

The variation in the distance of the centre of geometry (COG) of adsorbate molecules from the surface was calculated as

$$\rho(z) = \frac{\langle \Delta N_{z,z+\Delta z} \rangle}{L_x L_y \Delta z}, \quad (4)$$

where $\langle \Delta N_{z,z+\Delta z} \rangle$ is the ensemble average of the number of molecules whose centre of geometry is located in the region bound between z and z + Δz.

4. Radial density distribution (RDD)

The 2D-radial density distribution of N_2 molecules in the first layer was calculated from

$$\rho(r) = \frac{\langle \Delta N_{r,r+\Delta r} \rangle}{\pi[(r+\Delta r)^2 - r^2]}, \quad (5)$$

where $\langle \Delta N_{r,r+\Delta r} \rangle$ is the average number of particles whose centres of mass are located in the first layer and in the radial bin bounded by [r,r + Δr]. Δr was chosen as Δr = 0.01 nm.

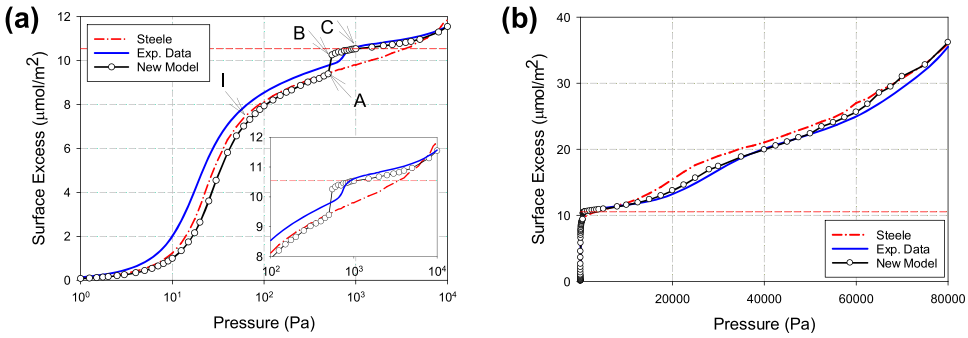

FIG. 4. GCMC simulated adsorption isotherm of N_2 at 77 K: comparison between the new model, 10-4-3, and experimental data:[9] (a) semi-log scale, (b) linear scale.

5. Orientational distribution

The mean orientation of N_2 molecules, defined as the angle between N_2 molecular axis and the normal vector from the graphite surface, was assessed by the distribution

$$\rho(z,\theta) = \frac{\langle \Delta N(z,\theta) \rangle}{L_x L_y \Delta z \sin\theta \Delta\theta}, \tag{6}$$

where $\langle \Delta N(z,\theta) \rangle$ is the average number of N_2 molecules whose centres of mass are located in the region bounded by [z, z + Δz] and an angle between the molecular axis and the z-direction within [θ,θ + Δθ]. Plots of $\rho(z,\theta)$ versus z and θ monitor the preferred orientation of the molecules located at various distances from the surface. A nitrogen molecule lying parallel to the surface is at an angle of θ = π/2 and one perpendicular to the surface is at an angle of zero.

III. RESULTS AND DISCUSSIONS

A. Nitrogen adsorption on graphite at 77 K

The experimental results for this system exhibit a number of interesting features in the isotherm and in the plots of isosteric heat versus loading and have been measured at sufficient resolution to allow us to discriminate between modeling with the 10-4-3 model and our new graphite model. Figure 4 shows the simulated and experimental adsorption isotherm for N_2 at 77 K on semilogarithmic and linear scales. The former emphasises the resolution at low loadings and the latter at higher loadings. At loadings below the monolayer coverage, the experimental result shows a 2D-transition from gas to liquid in the first layer (Fig. 4(a)), followed by a sub-step (transition) from the 2D supercritical state to a 2D commensurate solid. The continuum solid model fails to describe this transition (since there are no C hexagons with which N_2 can be commensurate), but the revised model clearly reproduces the sub-step from points A to B. Interestingly the density at point B is less than the theoretical commensurate density of 10.54 μmol/m^2 which would occur when the graphite surface is completely covered, with one N_2 molecule in registry for every three carbon hexagons. This state is only achieved after the sub-step has been completed because of an entropic

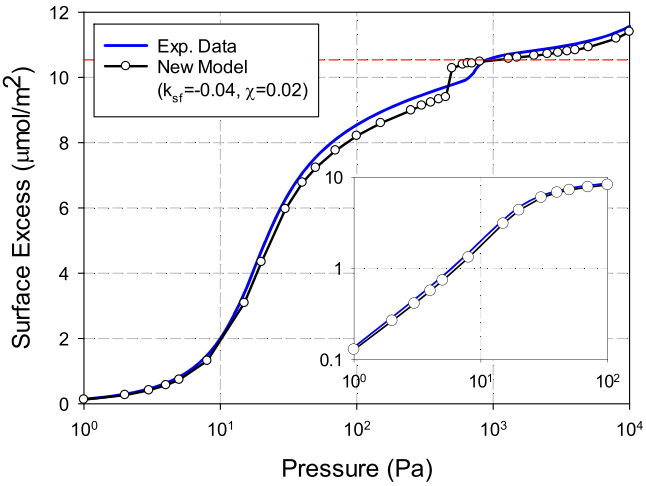

FIG. 5. GCMC simulated adsorption isotherm for N_2 at 77 K: comparison between the new model (k_{sf} = −0.04 and χ, of 0.02) and experimental data.[9] The inset is plotted on a log-log scale to show Henry's law region.

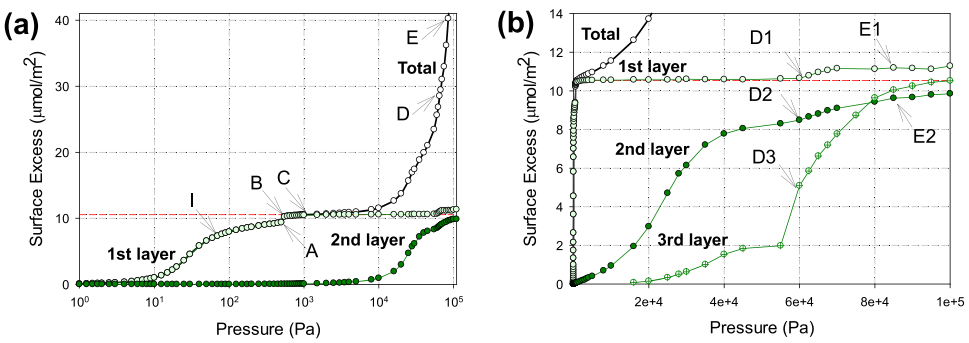

FIG. 6. GCMC simulated adsorption isotherm of N_2 at 77 K, obtained with the new model, decomposed into contributions from first and second layers: (a) semi-log scale, (b) linear scale. The first layer is bounded from 0 to 0.5 nm, the second layer from 0.5 to 0.8 nm, and the third layer from 0.8 to 1.15 nm based on the local density distribution LDD profile in Fig. 11. Points D1, D2, and D3 correspond to the first, second, and third layers' contribution of point D in Fig. 6(a) while points E1 and E2 correspond to the first and second layers' contribution of point E.

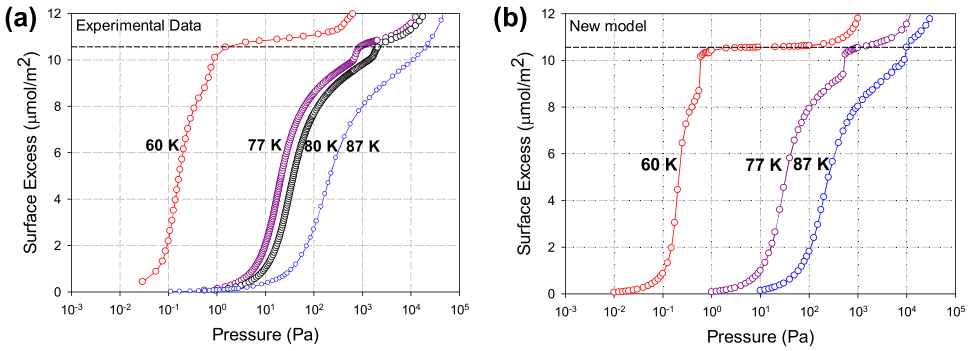

FIG. 7. (a) Experimental adsorption isotherm of N_2 Carbopack F (60, 77, and 80 K)[2] and on GCB-I (87 K)[36] in semi-log scale, (b) GCMC simulated adsorption isotherm of N_2 at various temperatures on a semi-log scale obtained with the revised model. The dashed line represents the commensurate density of 10.54 μmol/m^2.

disorder in the adsorbate. The new model is also able to describe the isotherm better in the multilayer region (Fig. 4(b)) where the 10-4-3 model overpredicts the amount adsorbed. This is simply because the 10-4-3 model has a more negative potential at the position of the higher layers, compared to the revised model (Fig. 3). In previous work, we accounted for three body mediation of the first layer nitrogen interaction by multiplying the well-depth for the SF interaction by a binary interaction parameter, k_{sf}, of −0.04 and making a reduction in the FF potential energy of 2% when two N_2 molecules are in the first layer.[8] The simulation results with these parameters show better agreement in Henry's law region as presented in Fig. 5. The importance of the anisotropy in the description of the substep in the isotherm is clear from the simulation results shown in the Appendix (Fig. 20) where the anisotropy has been omitted in the modeling and the transition from the 2D supercritical state to a 2D commensurate solid is absent which is inconsistent with the experimental data.

To understand how each layer contributes to the isotherm, we decomposed the isotherm into contributions from the first, second, and third layers (Fig. 6). At the substep (AB), the contribution from the second layer coverage is negligible, indicating that the sub-step is intrinsic to the first layer when it changes from a supercritical state to a commensurate state. The mechanism of this (AB) transition is as follows: the chemical potential at point B is high enough that more N_2 molecules can enter the first layer, which becomes more ordered, and the adsorbate molecules move closer to the energetically most favourable positions, at the centres of the carbon hexagons. Most of them are in registry with the graphene layer (see also Sections III B and III C). Because of these energetically favourable positions, the adsorbate in the first layer retains this configuration over a wide range of pressure until the multilayers formed on the surface provide sufficient fluid-fluid interaction energy to enable molecules in the first layer to move away from these positions—thereby decreasing their SF interactions—to form incommensurate 2D solids.

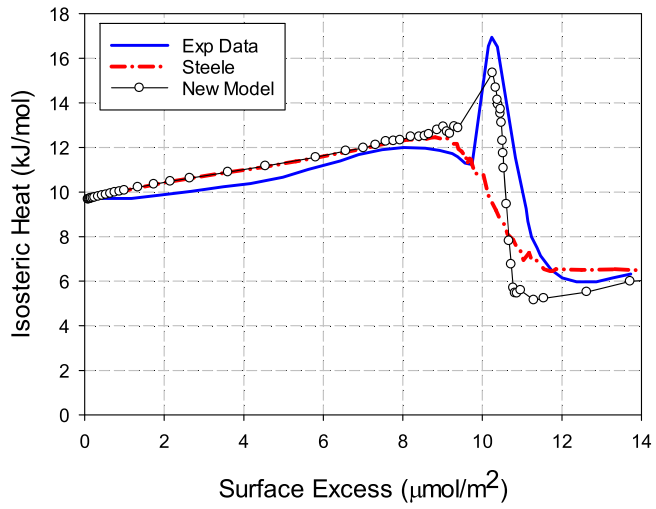

FIG. 8. GCMC simulated isosteric heat profile of N_2 adsorbed on graphite at 77 K obtained with the revised model compared with results obtained using the 10-4-3 continuum solid model and with experimental data from Grillet *et al.*[23]

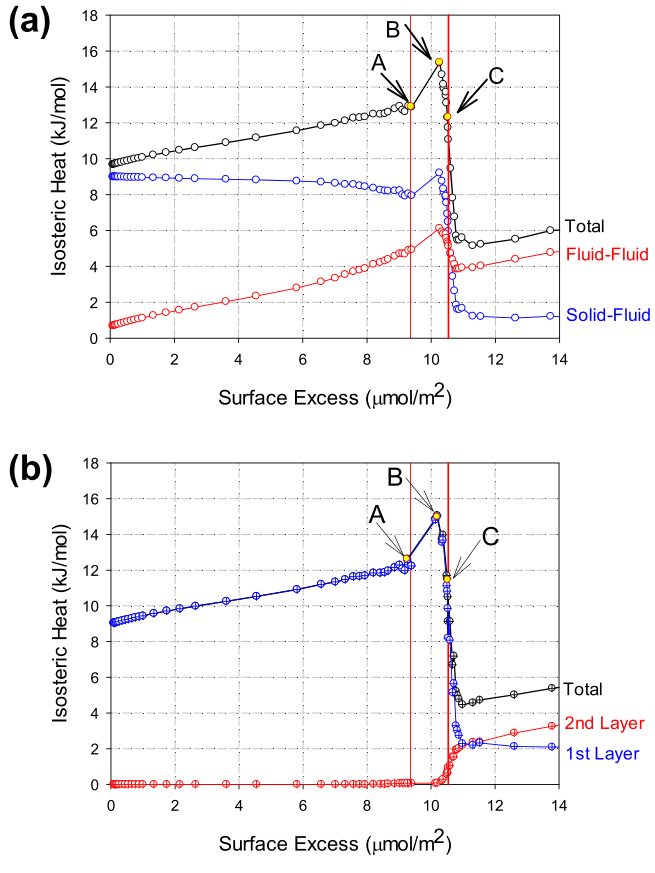

FIG. 9. GCMC simulated isosteric heat profile of N_2 adsorption on graphite at 77 K in comparison with experimental data from Grillet *et al.*: (a) new model decomposed into solid-fluid and fluid-fluid contribution, (b) new model decomposed into first and second layers' contribution. Points A-C correspond to the points marked in Fig. 6. Note: for (b), the k_BT term of 0.64 kJ/mol is excluded from the total isosteric heat and the sum of the first and second layer heats equals the total isosteric heat.

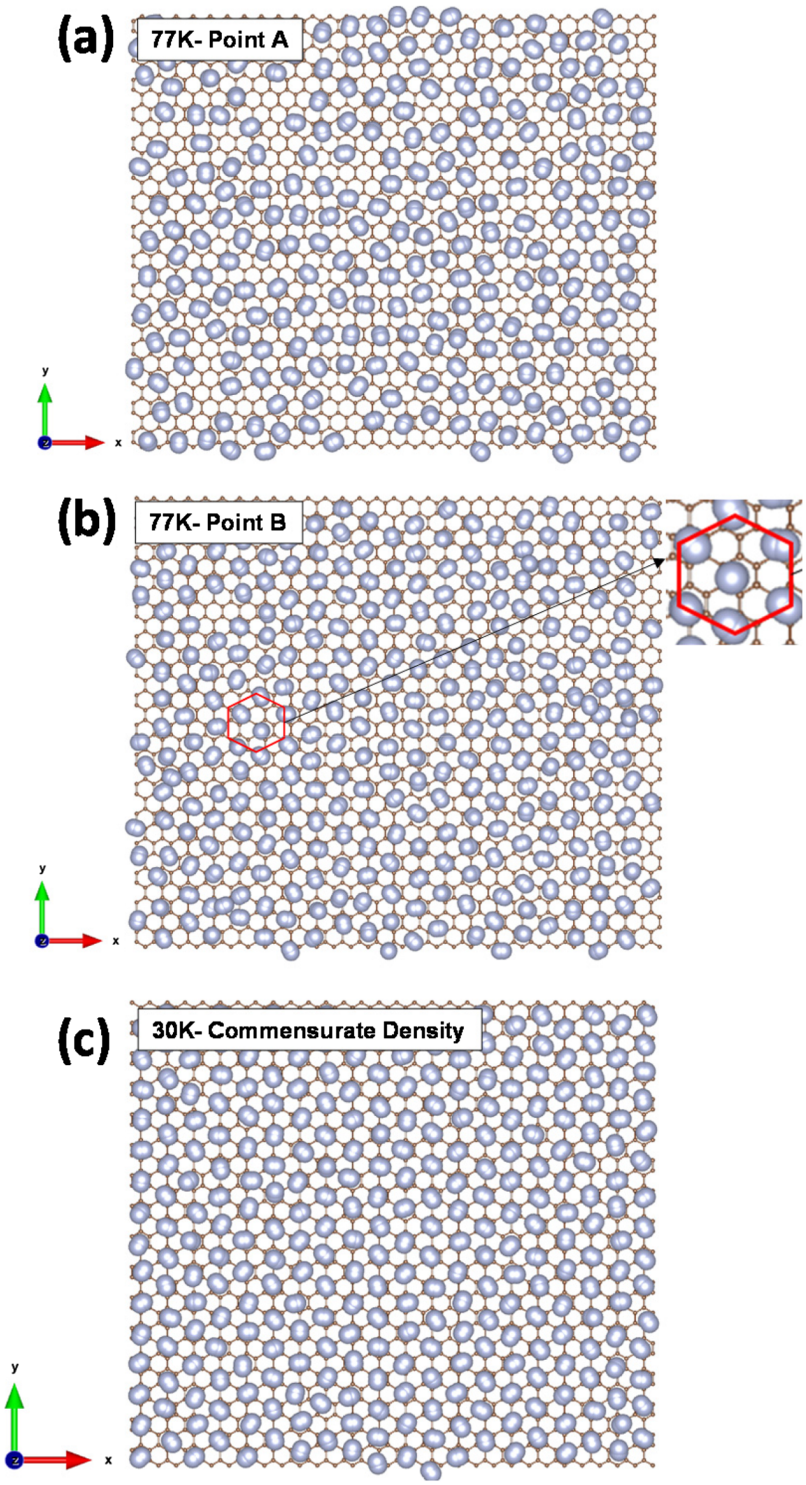

FIG. 10. GCMC simulation snapshot of N_2 molecules adsorbed on a graphite at 77 K obtained with the revised model: (a) before the substep (point A), (b) after (point B). (c) Snapshot at 30 K at the commensurate density of 10.54 μmol/m^2. The carbon lattice configuration was built based on the Kim and Steele potential[33] (detailed in the Appendix).

This marks the transition from point D1 to E1, which occurs after the 2nd and 3rd layers have been formed as shown in Fig. 6(b). These changes cannot be observed experimentally but serve to demonstrate the power of simulation in helping to unravel the detailed mechanisms underlying the experimental observation.

In Fig. 7(a) the experimental isotherms on Carbopack F (60, 77, and 80 K)[9] and on GCB-I (87 K)[37] show a more gradual transition compared to the simulated isotherms in Fig. 7(b). The magnitude of the sub-step decreases with increasing temperature and the sub-step is absent at 87 K where thermal fluctuation becomes dominant, and the higher layer is completed before the first layer. The discrepancy between simulation and experiment can be attributed to physical factors not accounted for in the model including the existence of very narrow pore spaces formed between the stacked micro-crystallites in Carbopack F and the distribution of crystallite size.

B. Isosteric heat

It has been reported in a previous publication[9] that the simulation of adsorbed N_2, using a diatomic model, on the

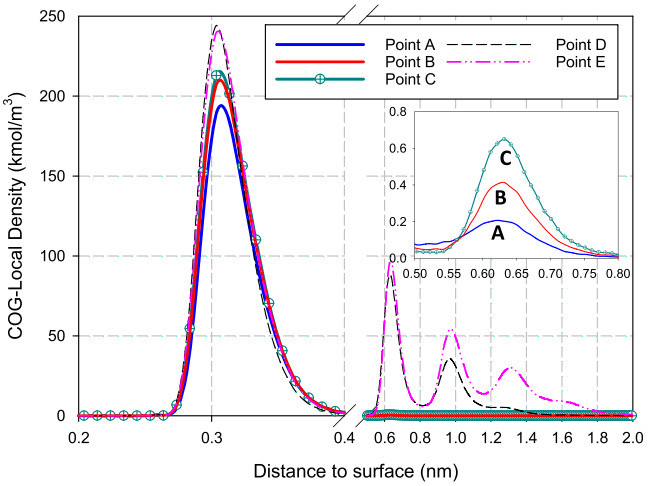

FIG. 11. COG local density distribution of N_2 adsorption on graphite obtained with GCMC simulation at 77 K at different loadings. Points A-E correspond to the points marked in Fig. 6(a). The inset shows the detail of the LDD in the higher layers.

surface of a structureless graphite fails to reproduce the heat spike and cusp observed experimentally at 77 K by Grillet *et al.* on a highly graphitized carbon.[23] Using the new graphite model proposed in this paper, we show in Fig. 8 the GCMC simulated isosteric heat versus loading together with the experimental data. Our simulation results from the new model are in good agreement with experiment, again confirming the role played by corrugation of the lateral potential enhanced by the anisotropy of the C polarisability. The simulation results do not exhibit the cusp observed experimentally at loadings between 8 and 10 μmol/m^2. This is observed at higher temperatures. This will be explained in Section III D.

To gain further insight on the behaviour of the isosteric heat versus loading, we decomposed the isosteric heat in two ways: (1) contributions from the SF and FF interactions and (2) contributions from the first and second layers.

1. Decomposition of isosteric heat profile

The contributions from SF and FF interactions to the isosteric heat are shown in Fig. 9(a). In the monolayer coverage region from zero loading to point A, the SF contribution slightly decreases with loading, and since in this region there is no contribution from the second layer this decrease must be attributed to the orientational change of N_2 molecules in the first layer. This is an entropic orientation effect, which is discussed more fully in Section III C. In this monolayer region, the FF contribution increases because of the increase in the average number of neighbouring molecules. Across the sub-step AB, both the FF and SF contributions increase and we see that the SF contribution at point B is the same as the SF interaction at zero loading where the FF contribution is zero, indicating that most of the molecules that penetrate the first layer adopt an orientation parallel to the surface in the same way as at zero loading. Snapshots of a configuration at points A and B are shown in Figs. 10(a) and 10(b), illustrating that the ordered array of molecules at point B is close to being in registry with the graphite surface. Complete registry only occurs at much lower temperatures (simulation at 30 K in Fig. 10(c)), as observed by Diehl and Fain from their LEED study.[38] Kuchta and Etters,[39] using an NpT MC technique, found that at this low temperature, the most favourable configuration occurs when two N_2 molecules lie at 90° to each other (i.e., in a T configuration) thereby maximising the quadrupole interaction. The 10-4-3 homogeneous solid model fails to describe the heat spike because corrugation is needed to lock N_2 molecules into a commensurate array with the graphite lattice.

Interestingly, the surface density at point B (at the end of the substep) is 10.25 μmol/m^2, which is less than the theoretical commensurate density of 10.54 μmol/m^2. Does this mean that as loading is further increased from the density of point B to the commensurate density the SF contribution should remain constant and the FF contribution increases because of an increase in the number of neighbours in the first layer? The simulation results however show opposite to what one would expect (Fig. 9). It is because of the entropic effects that incoming molecules favour the second layer adsorption as much as the first layer. This is an example of the balance between the energy and the entropy to minimize the free energy.

The argument that we put forward in the previous paragraph is corroborated when we analysed the contributions of the first and second layers to the isosteric heat (Fig. 9(b)). At point B, there is no contribution from the second layer to the isosteric heat, confirming our earlier assertion that the substep AB is intrinsic to the first layer. Recalling that the density at point B is slightly less than the theoretical commensurate (C) density, we consider point C on the isotherm at which the density is exactly the same as the C-density. At this point we begin to see the contribution from the second layer (Fig. 9(b)), which supports our explanation that there is a balance between energy and entropy, i.e., incoming molecules enter the system in the first layer as well as the second layer, resulting in a decrease in

TABLE II. Summary of layer contribution of surface excess and isosteric heat of GCMC simulated isosteric heats for N_2 adsorption on graphite at 77 K with the new model. Note: The total isosteric heat equals the sum of the isosteric heat of the first and second layers and k_BT of 0.64 kJ/mol.

			Total N of molecules			Isosteric heat (kJ/mol)		
Point	Pressure (Pa)	Surface excess (μmol/m^2)	Total	Layer 1	Layer 2	Total	Layer 1	Layer 2
A	450	9.26	263.00	262.10	0.87	13.27	12.56	0.07
B	550	10.14	288.06	286.91	1.12	15.52	14.80	0.07
C	950	10.52	298.84	296.78	2.06	12.14	10.82	0.68

both the SF and FF contributions as shown in Fig. 9(a) (from point B to C). This is further supported by the local density distribution at point C in the inset of Fig. 11, where molecules have begun to adsorb in the second layer. Table II summarizes the number of molecules in the first two layers and their contributions to the isosteric heat.

C. Local properties analysis

The conclusions derived in Sec. III B 1 can be substantiated by analysing the local density distribution of the centre of geometry (COG) of N_2 at various loadings, the 2D radial density distribution in the first layer, the 3D-orientational density distribution, and the commensurate packing function, $f(x, y)$, given in Subsection 1 of the Appendix.

1. Local density distribution (LDD)

The LDDs are presented in Fig. 11, where the first and the second layers are located at about 0.31 nm and 0.62 nm, from the graphite surface. The figure shows that before the onset of the second layer, there is a noticeable increase in density before and after the substep (point A to B) confirming that there is an increase in the number of N_2 neighbouring molecules to form commensurate packing in the first layer across the AB transition.

We consider the path DE on the isotherm (Fig. 6). Although it is not manifested clearly on the full isotherm, the corresponding increase in density D_1E_1 in the first layer isotherm shows a clear transition; this is the transition from commensurate packing to incommensurate packing in the first layer and occurs after the second and third layers are formed. Clearly neither the experimental nor the simulated total isotherm exhibits this transition, and it can only be observed by decomposing results from a computer simulation. To form an incommensurate packing, molecules have to shift away from the favourable positions on the surface (the centres of the carbon hexagon), which is associated with a decrease in the SF interaction. This SF energy decrease is compensated by an increase in the FF interactions from molecules in all layers, and the reason why the C-IC transition does not occur before the onset of the second layer is that the increase in FF contributions by molecules in the first layer is not sufficient to compensate for the decrease in the SF interaction.

2. 2D-radial density distribution

To demonstrate how molecules structure their registry with the graphite surface, we show in Fig. 12 the 2D-radial density distribution (2D-RDD) of the first layer. At point A, just before the substep, the radial distribution has a liquid-like pattern, characterized by single peaks separated by about one collision diameter. At the end of the substep (point B), peaks, with the exception of the first shell, become decorated with a shoulder. The positions of these peaks and shoulders correspond exactly to those of a perfect commensurate structure in registry with the graphite surface listed in Figure 13. Interestingly, the radial distribution at point E shows that the shoulders start to disappear and this indicates that molecules are no longer in registry with the graphite surface since the incoming molecules from higher layers force molecules in the first layer to sit closer to each other.

3. 3D-orientation distribution

To investigate how molecules in each layer orient with respect to a normal to the graphite surface, we consider the 3D-orientation density distributions in Fig. 14. At very low loadings nitrogen molecules adopt an orientation parallel to the surface plane (point I corresponds to loadings at a pressure of 70 Pa). At point A (before the substep) some molecules move towards vertical orientations which reduces the SF part of the isosteric heat in the sub-monolayer coverage

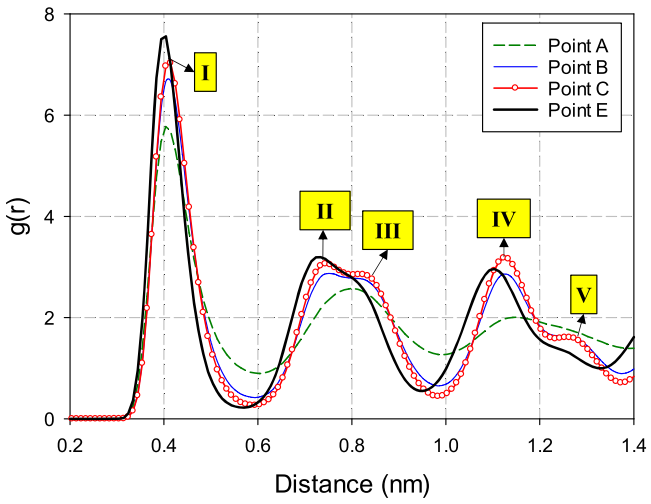

FIG. 12. 2D-radial density distribution of N_2 adsorption on graphite surface at 77 K. Points A-E correspond to the points marked in Fig. 6(a). Points I-V correspond to the marked region in Fig. 13.

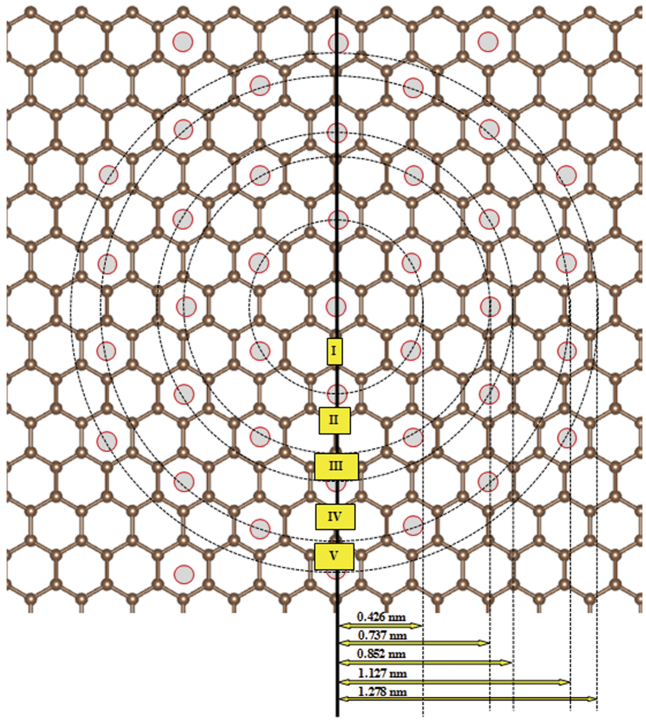

FIG. 13. A schematic radial distribution for a N_2 commensurate phase on a graphene plane.

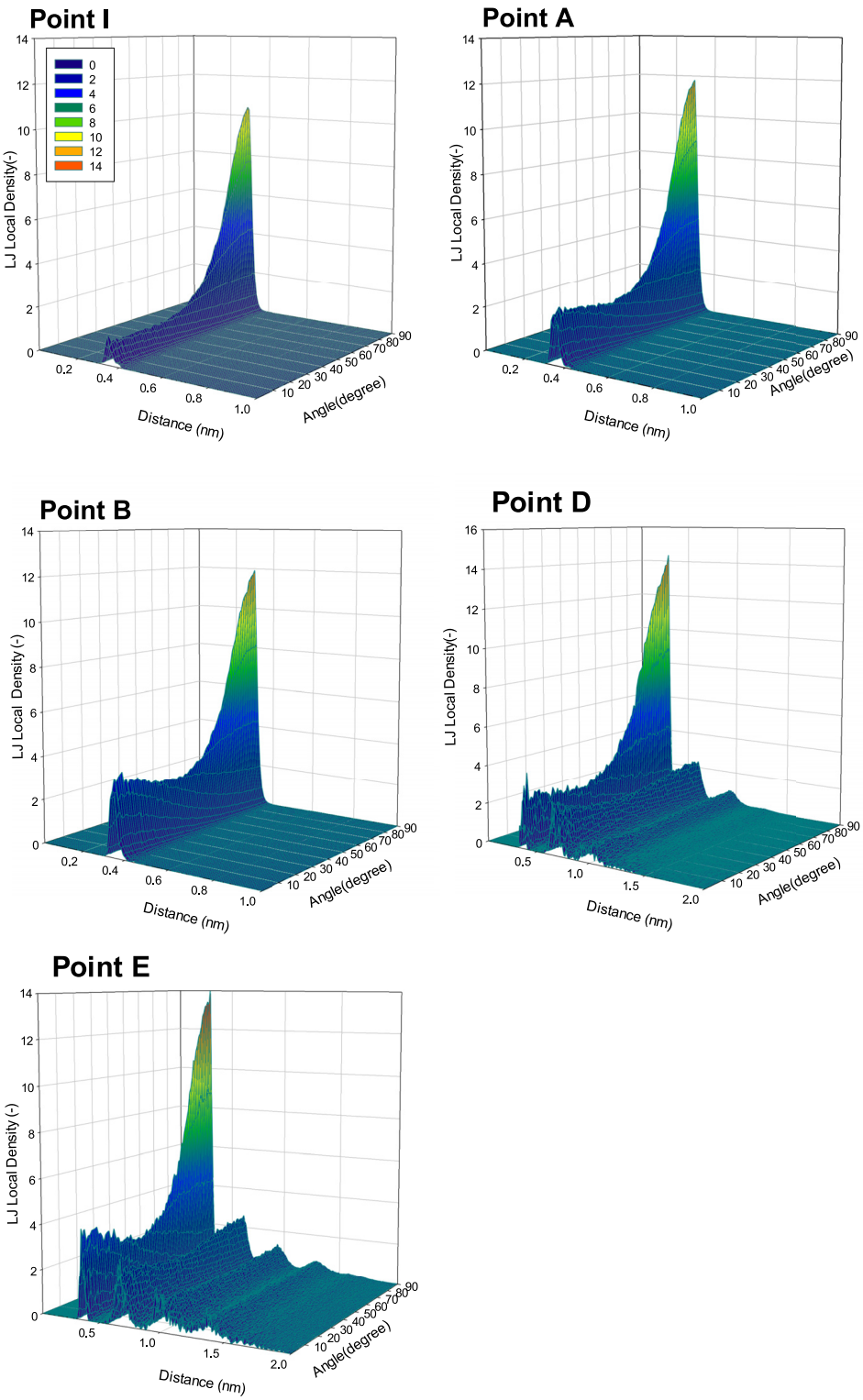

FIG. 14. 3D-orientation distributions from GCMC simulations of N_2 adsorbed at 77 K obtained with the new model at various loadings. Points A-E correspond to the points marked in Fig. 6.

region (Figure 9(a)). This may be attributed to the fact that some N_2 molecules reorient to maximise their intermolecular attraction. There is no observable difference between the orientation distribution at point B and that at point A demonstrating that molecules entering the first layer do not disturb the orientation of existing molecules. At point B, it can be seen that there is a higher population of N_2 molecules favouring the vertical orientation, and this configuration has contributions from both SF and FF interactions as previously discussed. Fig. 14 illustrates the distribution at point D where the second and higher layers have been formed, and here there is no preferred orientation because the adsorbent potential at this distance from the surface is too weak to structure the second layer. The orientational distribution at point E is more random than at point D, confirming that a C-IC transition has occurred. Fig. 15 shows the orientation distribution of N_2 molecules at the much lower temperature of 30 K where a perfect commensurate layer is formed. At this temperature, all the N_2 molecules

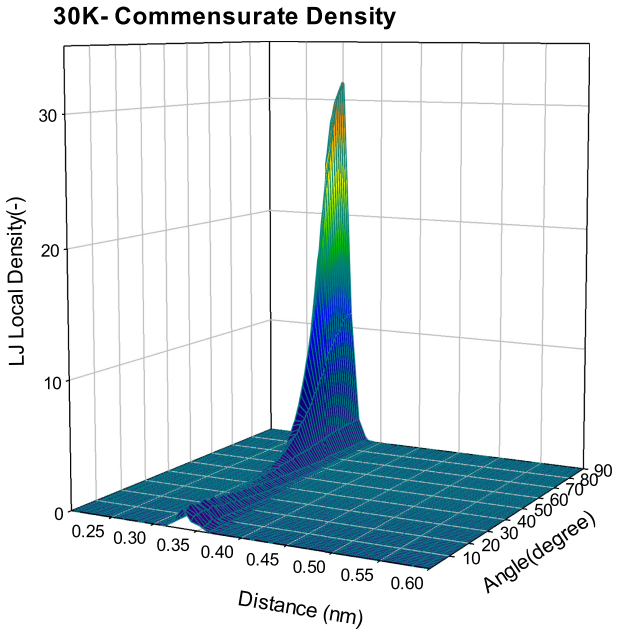

FIG. 15. 3D-orientation distribution from GCMC simulated N_2 adsorption at 30 K, using the new model, at the commensurate density.

adopt an orientation parallel to the surface, since the entropy contribution is very small.

4. Degree of commensurate packing—⟨g⟩

The function $f(x,y)$ in Eq. (A2) in the Appendix is a useful measure of the extent of commensurate packing. Here it is convenient to introduce a parameter $g = \langle -f(x,y)\rangle /2$ (the minus sign is introduced to make g positive) as first used by Jiang and co-workers.[40] When a molecule resides at the centre of the carbon hexagon, this parameter takes a value of 3. Fig. 16 shows the sharp increase in g across the transition AB, in keeping with a change in first layer from fluid-like ($g = 0.73$) to commensurate ($g = 1.53$). It is notable that the packing at point B is not perfectly commensurate (when g would be = 3) because it is disturbed by thermal fluctuation at 77 K. Simulation at 30 K shows that g has a value of 2.326 at the commensurate density. It was shown earlier that as higher layers form on the surface, the first layer goes through a transition from commensurate to incommensurate packing (D1 to E1 transition in Fig. 6(b)) and this is confirmed here by the decrease in the g factor.

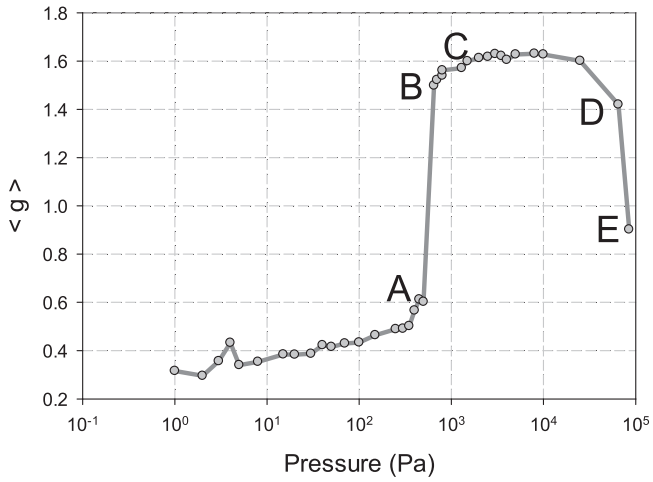

FIG. 16. Values of ⟨g⟩ against pressure for N_2 adsorption on graphite with the proposed model.

D. Effect of temperature

We show in Fig. 17 the different locations of the heat spike at different temperatures. As the temperature is increased, the position of the peak in the isosteric heat shifts to higher loadings. Interestingly, at 60 K, the SF contribution to the isosteric heat is nearly constant. This implies that most of the N_2 molecules are lying parallel to the surface, with very few in a vertical orientation. As temperature is increased, some more random orientations can occur and this is reflected in a steeper decline in the SF contribution to the heat below monolayer

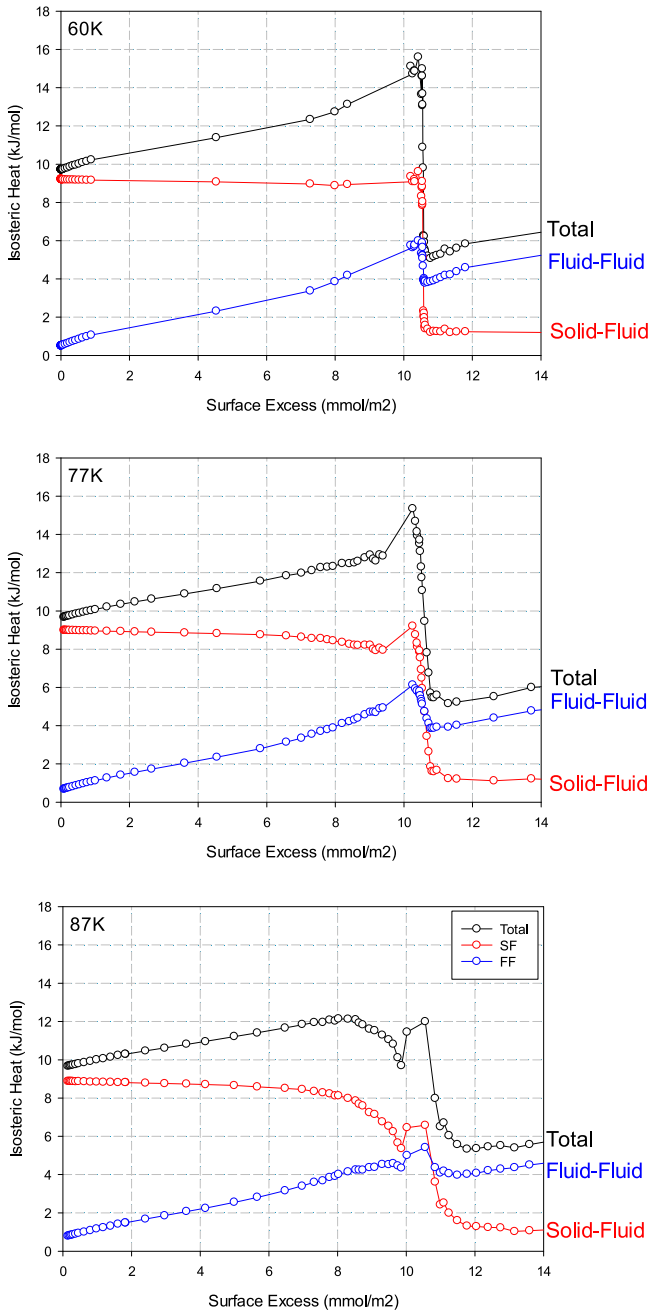

FIG. 17. GCMC simulated isosteric heat versus loading for N_2 adsorbed on graphite obtained with the revised model at 60 K, 77 K, and 87 K.

coverage. The decline in the SF isosteric heat is more distinct at 87 K due to the entropy effect and therefore the total isosteric heat profile shows a cusp similar to the one observed experimentally at 77 K. Our simulation result at 77 K does not show the cusp in the total isosteric heat and this could be due to the discrepancies between the temperature of the simulation and real experiment.

IV. CONCLUSION

The adsorption isotherms and isosteric heats of N_2 on graphite have been re-investigated using the GCMC simulation and data from the high-resolution experiment. We propose a new model that accounts for physical features of graphite that are often neglected: (1) the corrugation of the potential energy surface parallel to the graphene layers arising from the discrete atomic structure, (2) the difference between the polarizability of carbon parallel and normal to the graphene surface, and (3) the difference in separation between an outer graphene layer and that of the underlying layers, and the deeper well-depth of the potential energy of interaction. This new model improves the description of N_2 adsorption on graphite in accounting for the sub-step in the first layer of the isotherm, the spike in the isosteric heat curve versus loading and the adsorption at higher loading.

ACKNOWLEDGMENTS

This work is supported by the Australian Research Council (No. DP160103540).

APPENDIX: DETAILS OF THE NEW MOLECULAR MODEL FOR GRAPHITE

1. Kim and Steele's Fourier approximation for graphite surface

The summation of pairwise potential energies at any point $\underline{r}$ for graphite surface $\varphi(\underline{r})$ could be approximated by the laterally averaged potential and the Fourier approximation to account for the corrugation on the surface as described in Eq. (A1). $\varphi_0(z)$ is the laterally average potential, which is a function of z, the minimum distance from the site to the graphene layer. For graphite there are six equivalent vectors of magnitude of 29.5 nm^{-1}, whose contributions dominate the second term in the following equation:

$$\varphi(\underline{r}) = \varphi_0(z) + \varphi_g(z) f(x, y), \tag{A1}$$

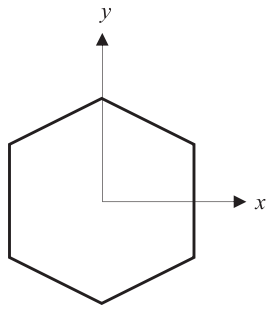

FIG. 18. Coordinate of graphite surface: the x-axis originates at the centre of a hexagon and bisects the carbon-carbon bond.

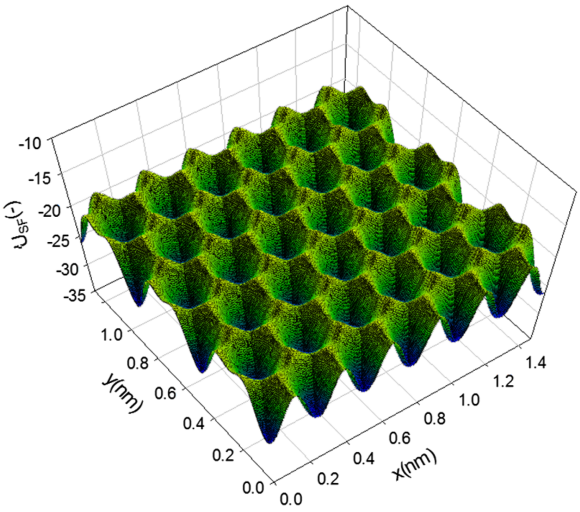

FIG. 19. Solid-fluid potential mesh plot of the corrugated graphite surface built using the revised new model.

where

$$f(x, y) = -2\left\{\cos(2\pi b_1) + \cos(2\pi b_2) + \cos\left[2\pi\left(b_1 + b_2\right)\right]\right\}. \tag{A2}$$

The minimum of this function occurs at the centre of the hexagon.[41] The x-axis originated from the centre of a hexagon and points towards a neighbouring carbon atom (Fig. 18), the parameters b_1 and b_2 are given by

$$b_1 = \frac{1}{a_{Gr}}\frac{2y}{\sqrt{3}}, b_2 = \frac{1}{a_{Gr}}\left(x - \frac{y}{\sqrt{3}}\right), \tag{A3}$$

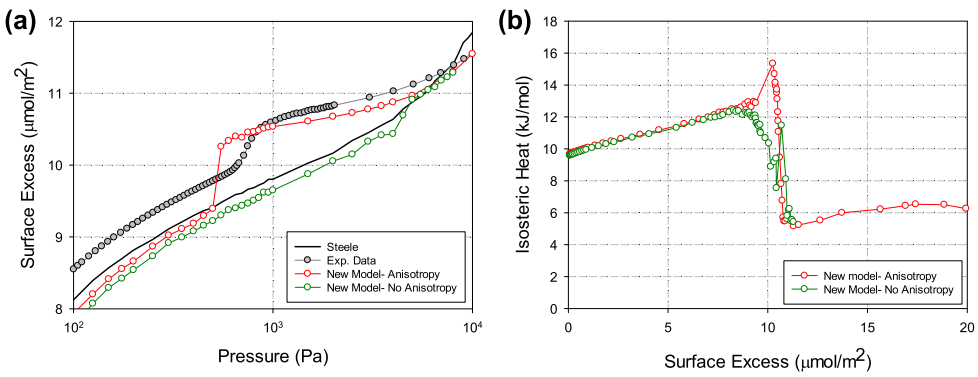

FIG. 20. GCMC simulated adsorption isotherm of N_2 at 77 K; comparison between the new model (with and without anisotropy), 10-4-3, and experimental data:[2] (a) adsorption isotherm, (b) isosteric heat profile.

where $a_{Gr} = d_{c-c}\sqrt{3} = (0.142\ \text{nm})\sqrt{3} = 0.246$ nm is the lattice constant of graphite and $d_{c-c} = 0.142$ nm is the length of the carbon-carbon bond.

For the uppermost Crowell surface (Fig. 1 in the main text), the laterally average potential is

$$\varphi_0(z) = 2\pi\left(\sigma^2\rho\right)\varepsilon\left[\frac{2}{5}\left(\frac{\sigma}{z}\right)^{10} - \left(\frac{\sigma}{z}\right)^4\right], \tag{A4}$$

where ρ is the surface carbon atom density of a graphene layer ($38.2\ \text{nm}^{-2}$), σ is the solid-fluid collision diameter, and ε is the solid-fluid interaction energy calculated from the Lorentz-Berthelot mixing rule with $\sigma_{CC} = 0.28$ nm and $\varepsilon_{CC}/k = 35\ K$.

The functional form of $\varphi_g(z)$ is[33]

$$\varphi_g(z) = 2\pi\left(\sigma^2\rho\right)\varepsilon\left[\left(\frac{16\pi^5}{30}\right)\left(\frac{\sigma}{d_0}\right)^5\left(\frac{\sigma}{z}\right)^5 K_5\left(\frac{4\pi z}{d_0}\right) - 4\pi^2\left(\frac{\sigma}{d_0}\right)^2\left(\frac{\sigma}{z}\right)^2 K_2\left(\frac{4\pi z}{d_0}\right)\right]. \tag{A5}$$

In the presence of anisotropy, Carlos and Cole[27] presented the following equation:

$$\varphi_g(z) = 2\pi\left(\sigma^2\rho\right)\varepsilon\left\{\left(\frac{16\pi^5}{30}\right)\left(\frac{\sigma}{d_0}\right)^5\left(\frac{\sigma}{z}\right)^5\left[K_5\left(\frac{4\pi z}{d_0}\right) + \gamma_R g_R(z)\right] - 4\pi^2\left(\frac{\sigma}{d_0}\right)^2\left(\frac{\sigma}{z}\right)^2\left[K_2\left(\frac{4\pi z}{d_0}\right) + \gamma_A g_A(z)\right]\right\}, \tag{A6}$$

where $d_0 = a_{Gr}\sqrt{3} = 0.426$ nm, which is the lattice spacing of the $(\sqrt{3}\times\sqrt{3})R30$ structure. The functions K5 and K2 are the Bessel functions of the second kind. As previously mentioned in the main text, we adopted values of $\gamma_A = 0.4$ and $\gamma_R = -1.05$ from Joshi and Tildesley.[42] Fig. 19 shows the solid-fluid potential mesh plot of the graphite surface built using the revised new model (Fig. 1 in the main text), where the minimum occurs at the centre of a hexagon. The comparison of adsorption isotherm and isosteric heat profile in the presence and absence of anisotropy is shown in Fig. 20.

[1] W. A. Steele, "The physical interaction of gases with crystalline solids: I. Gas-solid energies and properties of isolated adsorbed atoms," Surf. Sci. **36**(1), 317–352 (1973).

[2] A. Wongkoblap, D. D. Do, and D. Nicholson, "Explanation of the unusual peak of calorimetric heat in the adsorption of nitrogen, argon and methane on graphitized thermal carbon black," Phys. Chem. Chem. Phys. **10**(8), 1106–1113 (2008).

[3] C. Fan, M. A. Razak, D. D. Do, and D. Nicholson, "On the identification of the sharp spike in the heat curve for argon, nitrogen, and methane adsorption on graphite: Reconciliation between computer simulation and experiments," J. Phys. Chem. C **116**(1), 953–962 (2012).

[4] V. T. Nguyen, D. D. Do, and D. Nicholson, "On the heat of adsorption at layering transitions in adsorption of noble gases and nitrogen on graphite," J. Phys. Chem. C **114**(50), 22171–22180 (2010).

[5] D. Do and H. Do, "Evaluation of 1-site and 5-site models of methane on its adsorption on graphite and in graphitic slit pores," J. Phys. Chem. B **109**(41), 19288–19295 (2005).

[6] L. Prasetyo, T. Horikawa, P. Phadungbut, S. J. Tan, D. Do, and D. Nicholson, "A GCMC simulation and experimental study of krypton adsorption/desorption hysteresis on a graphite surface," J. Colloid Interface Sci. **478**, 402–412 (2016).

[7] R. Diao, C. Fan, D. D. Do, and D. Nicholson, "On the 2D-transition, hysteresis and thermodynamic equilibrium of Kr adsorption on a graphite surface," J. Colloid Interface Sci. **460**, 281–289 (2015).

[8] D. Do and H. Do, "Adsorption of quadrupolar, diatomic nitrogen onto graphitized thermal carbon black and in slit-shaped carbon pores. Effects of surface mediation," Adsorpt. Sci. Technol. **23**(4), 267–288 (2005).

[9] C. Fan, D. Do, D. Nicholson, J. Jagiello, J. Kenvin, and M. Puzan, "Monte Carlo simulation and experimental studies on the low temperature characterization of nitrogen adsorption on graphite," Carbon **52**, 158–170 (2013).

[10] D. Do and H. Do, "Effects of potential models on the adsorption of carbon dioxide on graphitized thermal carbon black: GCMC computer simulations," Colloids Surf., A **277**(1), 239–248 (2006).

[11] D. Do and H. Do, "Adsorption of benzene on graphitized thermal carbon black: Reduction of the quadrupole moment in the adsorbed phase," Langmuir **22**(3), 1121–1128 (2006).

[12] D. Do and H. Do, "Effects of potential models on the adsorption of ethane and ethylene on graphitized thermal carbon black. Study of two-dimensional critical temperature and isosteric heat versus loading," Langmuir **20**(25), 10889–10899 (2004).

[13] L. Prasetyo, D. Do, T. Horikawa, K. Nakai, and D. Nicholson, "On the resolution of constant isosteric heat of propylene adsorption on graphite in the sub-monolayer coverage region," Colloids Surf., A **512**, 101–110 (2017).

[14] D. Do and H. Do, "Adsorption of carbon tetrachloride on graphitized thermal carbon black and in slit graphitic pores: Five-site versus one-site potential models," J. Phys. Chem. B **110**(19), 9520–9528 (2006).

[15] D. Do and H. Do, "Adsorption of flexible n-alkane on graphitized thermal carbon black: Analysis of adsorption isotherm by means of GCMC simulation," Chem. Eng. Sci. **60**(7), 1977–1986 (2005).

[16] V. T. Nguyen, D. Do, D. Nicholson, and J. Jagiello, "Effects of temperature on adsorption of methanol on graphitized thermal carbon black: A computer simulation and experimental study," J. Phys. Chem. C **115**(32), 16142–16149 (2011).

[17] G. Birkett and D. Do, "Simulation study of methanol and ethanol adsorption on graphitized carbon black," Mol. Simul. **32**(10-11), 887–899 (2006).

[18] G. Birkett and D. Do, "Simulation study of ammonia adsorption on graphitized carbon black," Mol. Simul. **32**(7), 523–537 (2006).

[19] W. A. Steele, "The interaction of rare gas atoms with graphitized carbon black," J. Phys. Chem. **82**(7), 817–821 (1978).

[20] J. Rouquerol, S. Partyka, and F. Rouquerol, "Calorimetric evidence for a bidimensional phase change in the monolayer of nitrogen or argon adsorbed on graphite at 77 K," J. Chem. Soc., Faraday Trans. 1 **73**, 306–314 (1977).

[21] M. Kruk, Z. Li, M. Jaroniec, and W. R. Betz, "Nitrogen adsorption study of surface properties of graphitized carbon blacks," Langmuir **15**(4), 1435–1441 (1999).

[22] J. P. Olivier, "Chapter seven—The surface heterogeneity of carbon and its assessment," in *Adsorption by Carbons* (Elsevier, Amsterdam, 2008), pp. 147–166.

[23] Y. Grillet, F. Rouquerol, and J. Rouquerol, "Two-dimensional freezing of nitrogen or argon on differently graphitized carbons," J. Colloid Interface Sci. **70**(2), 239–244 (1979).

[24] J. J. Potoff and J. I. Siepmann, "Vapor–liquid equilibria of mixtures containing alkanes, carbon dioxide, and nitrogen," AIChE J. **47**(7), 1676–1682 (2001).

[25] E. A. Ustinov, "Effect of crystallization and surface potential on the nitrogen adsorption isotherm on graphite: A refined Monte Carlo simulation," Carbon **100**, 52–63 (2016).

[26] W. E. Carlos and M. W. Cole, "Anisotropic He–C pair interaction for a He atom near a graphite surface," Phys. Rev. Lett. **43**(10), 697 (1979).

[27] W. E. Carlos and M. W. Cole, "Interaction between a He atom and a graphite surface," Surf. Sci. **91**(1), 339–357 (1980).

[28] V. V. Gobre and A. Tkatchenko, "Scaling laws for van der Waals interactions in nanostructured materials," Nat. Commun. **4**, 2341 (2013).

[29] A. Crowell, "Approximate method of evaluating lattice sums of r—n for graphite," J. Chem. Phys. **22**(8), 1397–1399 (1954).

[30] M. W. Cole and J. R. Klein, "The interaction between noble gases and the basal plane surface of graphite," Surf. Sci. **124**(2-3), 547–554 (1983).

[31] D. Do, D. Nicholson, and H. Do, "On the Henry constant and isosteric heat at zero loading in gas phase adsorption," J. Colloid Interface Sci. **324**(1), 15–24 (2008).

[32] D. Whitehouse and A. Buckingham, "Experimental determination of the atomic quadrupole moment of graphite," J. Chem. Soc., Faraday Trans. **89**(12), 1909–1913 (1993).

[33] H.-Y. Kim and W. Steele, "Computer-simulation study of the phase diagram of the CH_4 monolayer on graphite: Corrugation effects," Phys. Rev. B **45**(11), 6226 (1992).

[34]D. Nicholson, "First order dispersion energy in the interaction of small molecules with graphite," Surf. Sci. **146**(2-3), 480–500 (1984).
[35]D. Nicholson, "Graphite polarizability," Surf. Sci. **181**(3), L189–L192 (1987).
[36]D. Nicholson and G. Parsonage, *Computer Simulation and The Statistical Mechanics of Adsorption* (Academic Press, London, 1982).
[37]K. Nakai, Y. Nakada, M. Hakuman, M. Yoshida, Y. Senda, Y. Tateishi, J. Sonoda, and H. Naono, "High resolution N_2 adsorption isotherms at 77.4 K and 87.3 K by carbon blacks and activated carbon fibers–Analysis of porous texture of activated carbon fibers by αs-method," J. Colloid Interface Sci. **367**(1), 383–393 (2012).
[38]R. D. Diehl and S. C. Fain, "Structure and orientational ordering of nitrogen molecules physisorbed on graphite," Surf. Sci. **125**(1), 116–152 (1983).
[39]B. Kuchta and R. Etters, "Calculated properties of monolayer and multilayer N_2 on graphite," Phys. Rev. B **36**(6), 3400 (1987).
[40]S. Jiang, K. E. Gubbins, and J. A. Zollweg, "Adsorption, isosteric heat and commensurate-incommensurate transition of methane on graphite," Mol. Phys. **80**(1), 103–116 (1993).
[41]M. L. Klein, S. O'Shea, and Y. Ozaki, "Interaction potentials and the properties of xenon overlayers physisorbed on the graphite basal plane," J. Phys. Chem. **88**(7), 1420–1425 (1984).
[42]Y. Joshi and D. Tildesley, "A simulation study of the melting of patches of N_2 adsorbed on graphite," Mol. Phys. **55**(5), 999–1016 (1985).